Slider-Tendon Linear Actuator With Under-Actuation and Fast-Connection for Soft Wearable Robots

Byungchul Kim, *Member, IEEE*, Useok Jeong, Brian Byunghyun Kang, *Member, IEEE*, and Kyu-Jin Cho, *Member, IEEE*

***Abstract*—Tendon-driven soft wearable robots should be simple, compact, and safe because they are worn on the human body and interact directly with the human. Here, unlike rigid robots, wire pre-tension should be removed at the end-effector due to the inherent characteristics of the soft robot. In this article, for a stable and compact actuation system without pretension, a linear actuator called a slider-tendon linear actuator is proposed. The proposed actuator is designed to make a linear motion using a tendon, as compared to other linear transmissions, such as ball screw or lead screw transmissions. By using the proposed design method that uses a tendon, the actuator size was reduced to 23.6% of the size of an actuator that uses a ball screw; this is because the tendon can endure high tensile force with a small cross-section area. Furthermore, this article proposes a robot design methodology to locate the robot mechanism in the actuator, rather than in the end-effector. The proposed actuator is designed to contain a fast-connection and stroke-amplified under-actuation mechanism. In the proposed method, not only is the complexity and size of the worn part reduced, but its performance is also improved. Finally, by applying this actuator to a specific wearable robot, this paper verifies that the proposed actuator sufficiently satisfies the requirements of the wearable robot.**

***Index Terms*—Soft wearable robot, tendon connector, tendon-driven actuator, under-actuation mechanism, tendon transmission.**

Manuscript received August 12, 2020; revised November 17, 2020; accepted December 30, 2020. Date of publication January 5, 2021; date of current version December 15, 2021. Recommended by Technical Editor C. Liu and Senior Editor W. J. Chris Zhang. This work was supported by a National Research Foundation of Korea Grant funded by the Korean Government under Grant NRF-2016R1A5A1938472, Grant 2015M3C1B2052817, and Grant 2019R1F1A1041277. *(Corresponding author: Kyu-Jin Cho.)*

Byungchul Kim, Brian Byunghyun Kang, and Kyu-Jin Cho are with the Biorobotics Laboratory, School of Mechanical Engineering, Soft Robotics Research Center, SNU-IAMD, Institute of Engineering Research, Seoul National University, Seoul 08826, South Korea (e-mail: kbc1990@snu.ac.kr; bbk8@cornell.edu; kjcho@snu.ac.kr).

Useok Jeong is with the Applied Robot R&D Department, Korea Institute of Industrial Technology, Ansan-si 31056, South Korea (e-mail: snopyy@snu.ac.kr).

This article has supplementary material provided by the authors and color versions of one or more figures available at https://doi.org/10.1109/TMECH.2020.3048962.

Digital Object Identifier 10.1109/TMECH.2020.3048962

I. Introduction

TENDON transmissions have advantages in their ability to make the end-effector of a robot compact, simple, and safe, as compared to other transmissions, such as linkage or gear transmissions [1], [2]. Tendon transmissions allow heavy components, such as the actuator, controller, and battery—to be located far from the end-effector through the use of a simple structure, such as the Bowden cable shown in Fig. 1. Therefore, tendon transmissions have been widely used in soft wearable robots designed for disabled people with difficulties in daily life [3], patients in need of rehabilitation [4], [5], soldiers in extreme environments [6], and tired workers who have difficulty maintaining their posture [7]. In these applications, soft wearable robots benefit from a simple, compact, and light end-effector because rigid, heavy, and bulky components (e.g., actuators and controllers) can be located far from the end-effector and, thus, can be more easily carried [8]–[11].

To implement tendon transmissions in soft wearable robots, method is to pull and release the wire through a linear motion [12], [13]. A ball screw is commonly used because it has high back-drivability, reliability, and accuracy. However, the actuator becomes bulky when the required stroke is long because the traveling length of the linear component must be longer than the stroke of the wire. Furthermore, if the required tension increases, the actuator becomes even bulkier due to the enlargement of the ball screw mechanism and the resulting increase in the cross-sectional area. Also, a ball screw can be excessive in a tendon transmission with a Bowden cable, because the tendon can only transmit the tensile force. Further, the friction of the Bowden cable degrades the advantage of the ball screw actuator (i.e., back-drivability, reliability, and accuracy).

As an alternative design, to minimize the size of the actuator, a spool-driven method can be used [14]–[17]. In this setup, the wire is pulled by winding it around a spool that is connected to a rotary motor. In this case, the derailment of the wire around the spool can induce tangling failure. One way of preventing derailment is to use antagonistic actuation with pretension; this approach is widely used for traditional rigid robots [13], [18], [19]. In the soft robotic field, unfortunately, pretension could cause unwanted deformation of the structure. Therefore, the actuation could cause unwanted side effects, such as unwanted motion and reduced efficiency [20], [21]. Recently, several

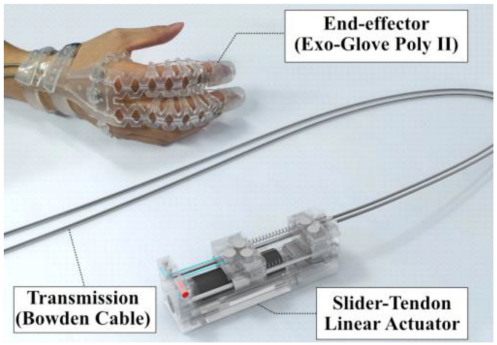

Fig. 1. Soft wearable robot application using the slider-tendon linear Actuator. The proposed actuator provides adaptability and usability to the soft wearable robot by including functions, such as fast-connection, under-actuation mechanism, and stroke amplification.

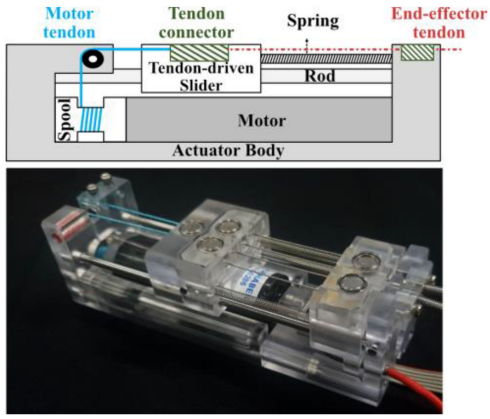

Fig. 2. Basic concept (up) and overview (bottom) of the proposed actuator. With a tendon-driven slider, the actuator could be designed in compact size and have reliable actuation performance. The proposed actuator pulls the end-effector tendon (red dotted line) by winding the motor tendon (blue solid line) that pulls the slider. In the release process of the end-effector tendon, the spool unwinds the motor tendon and springs pull the slider and motor tendon.

soft wearable robots adopted an actuation method that uses a slack-enabling mechanism that incorporates rollers to prevent derailment, without applying pretension on the robot [3], [5], [20], [21]. Rollers sustain only the tension of the tendon inside the actuator (not the whole tendon) by applying friction on the tendon. Here, a wire is divided by rollers into two sections: a pretension section inside the actuator and a tension-free section outside the actuator. However, since the friction and slip between the wire and rollers are used for stable actuation, researchers are still struggling to overcome the low durability of the wire and rollers [17].

In wearable robot applications, both the size and reliability of the actuator are important factors that affect the performance of the wearable robot. The reliability of the actuator system affects the safety of the robot users, while the size affects portability and usability [8]. A ball screw is reliable, accurate, and back drivable; however, the size is bulky. On the other hand, a slack-enabling actuator is compact, but it is not reliable or efficient, because the mechanism utilizes the friction and slip between the wire and rollers. This size and reliability issue of the tendon-driven soft wearable robots comes from the fact that the tendon connected to the motor and the tendon at the end effector have different requirements. Tension of the tendon connected to the motor has to be sustained because of derailment, while the tension of the tendon at the end-effector has to be removed when the robot is not operating.

In this article, we propose a linear actuator that uses a tendon-driven slider that decouples a tendon into two parts: a motor tendon and an end-effector tendon, as shown in Fig. 2. In this design, each side of the slider is connected to two different tendons. When the motor winds the motor tendon around the spool, the motor tendon pulls the slider. Then, the slider pulls the end-effector tendon that is connected to the end-effector. In this step, the slider also elongates the springs that are installed parallel to the end-effector tendon. In the unwinding process, on the other hand, wire derailment at the spool is prevented by the restoring motion of the elongated springs. The tendon-driven slider with two springs and two separate tendons (i.e., the motor tendon and the end-effector tendon) offer the following contributions.

1) This design reduces actuator size, as compared to a ball screw linear actuator. It has a small cross-sectional area since the tendon is strong at resisting a tensile force. However, the Slider-tendon linear actuator can only generate a force in the direction of pulling the end-effector tendon. The fact that the slider can only generate force in a single direction is not a problem in a tendon transmission, because the transmission only can transmit the tensile force.
2) The proposed approach has better aspects in terms of reliability and durability, as compared to the use of a slack-enabling mechanism. By connecting springs serial to the motor tendon but parallel to the end-effector tendon, the tension of the motor tendon can be sustained without tensioning the end-effector tendon. The proposed design applies only tension on the wire while the slack-enabling mechanism applies friction on the wire for the operation.
3) The use of the slider enables the addition of other features [8] that improve maintenance, efficiency, operability, and portability of wearable robots. As shown in Fig. 3, without increasing the size or complexity of the actuator system, the slider-tendon transmission contains the following features in a single actuation unit: an underactuation mechanism that enhances the simplicity and adaptability of the robot without complex control; a fast-connection that increases portability and eases maintenance; and a stroke amplification method that helps to keep the size of the actuator small, while generating a long wire stroke. Further details regarding each of these actuator features are explained in the following section.

As a result of utilizing the tendon-driven slider, the size of the proposed actuator is reduced to 23.6% of the size of a ball screw linear actuator. Furthermore, derailment prevention with a spring, rather than rollers, increases the reliability and durability of the actuation system. These increases are enabled because the tensile force is applied on the wire, rather than friction and slip. Containing other functions—such as under-actuation,

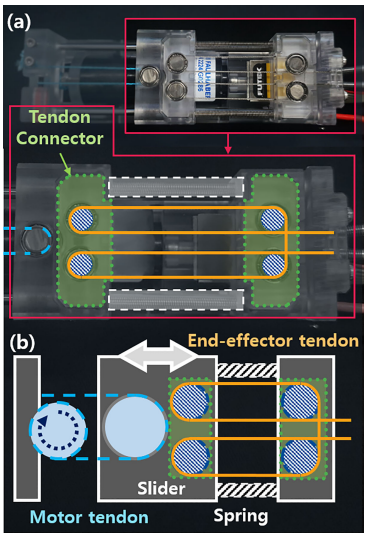

Fig. 3. Details of the proposed actuator working principles. The actuator offers the following four functions in a single slider. (a) Derailment of the motor tendon is prevented by springs (white broken line). (B) Underactuation is implemented to the end-effector tendon using a movable pulley in the slider (dark blue hatched circle). (c) The fast-connection makes the end-effector separate from the actuator easily (green dotted line). (d) The stroke of the tendon is amplified by designing the tendon path with movable pulleys (yellow solid line).

fast-connection, and the stroke amplification mechanism—in the actuator, rather than in the end-effector, not only reduces the complexity of the end-effector, but also improves the performance of the functions. Since these functions are located in the actuator, useful mechanical components can be used that might otherwise not be available in the end-effector due to the desire to not to harm the simplicity, softness, and usability of the end-effector. Details of the actuator design and contribution are described in the following order.

The rest of this article is organized as follows. Section II provides details about how the slider-tendon transmission is designed and how the additional features are included in the actuator. After this explanation of the slider-tendon transmission, a detailed design process is explained in Section III to inform a method to decide mechanical components. Also, this section shows how the proposed actuator could be used in a specific robot. Here, a previously designed robot named Exo-Glove Polly II is used. Next, Section IV shows the performance of the actuator and the simulation result. Finally, Section V concludes this article.

II. Working Principle of the Actuator

This section explains the working principle of the slider-tendon linear actuator. The actuator contains the four major functions to satisfy the requirements of the actuator needed for a soft wearable robot. In addition, since these functions can all be implemented through a single linear motion, the size of the actuator does not increase, as shown in Fig. 3. This section explains the methods used to implement each feature listed below, including the wire derailment prevention mechanism, the under-actuation mechanism, the fast-connection mechanism, and the stroke amplification mechanism.

A. Wire Derailment Prevention Mechanism

For derailment prevention, internal springs [white, broken line in Fig. 3(a)] are installed in the Slider-Tendon linear actuator. The main principle of derailment prevention is to connect the spring at the middle of the tendon. Using this connection method, some part of the tendon, the tendon that will be wound around the spool, is connected in series with the spring; the other part is connected in parallel with the spring. Since the pretension of the spring only affects the serially connected tendon, it is possible to make an actuator that prevents derailment at the spool without applying pretension on the end-effector. The tendon-driven slider is the main component that connects the spring, as noted above; The slider divides the wire into the motor tendon [blue, broken line in Fig. 3(b)] and the end-effector tendon [yellow, solid line in Fig. 3(b)]. The motor tendon only exists inside the actuator and the end-effector tendon is connected both to the end-effector and to the actuator. When the spool winds the motor tendon, the slider moves toward the spool and the internal spring elongates. In the unwinding step, the internal spring pulls the slider and the motor tendon back in the opposite direction. Therefore, the spring works to prevent the motor tendon from losing tension, even in the unwinding process. Note that the springs are attached in parallel to the end-effector tendon; thus, the spring compliance does not affect the compliance of the actuation unlike series elastic actuators [22], [23].

The tendon-driven slider, a component used to apply pretension on the motor tendon, not only decouples the tendon, but also serves as a transmission, which affects the tension and linear speed of the end-effector tendon. The relation between the motor dynamics and the end-effector tendon dynamics can be described by the following equations:

$$T_{\text{endeffector}} = \frac{n_m \varepsilon_M}{n_e R}\,\tau_M - kx = (\varepsilon\varepsilon_M)\,\tau_M - kx \quad (1)$$

$$V_{\text{endeffector}} = \frac{n_e R}{n_m \varepsilon_M}\,w_M = (\varepsilon\varepsilon_M)^{-1} w_M \quad (2)$$

$$\tau_{\text{impact}} = \frac{n_e R}{n_m} F_{\text{impact}} = \varepsilon^{-1} F_{\text{impact}} \quad (3)$$

where $T_{\text{endeffector}}$, $V_{\text{endeffector}}$, and τ_{impact} represent the tension of the end-effector tendon, the velocity of the end-effector tendon, and the impact applied to the motor, respectively. Since the spring is connected to the actuation unit, the tension produced by the motor results in a loss as much as the elastic force, as expressed in (1). Also, it is possible to prevent the motor from being broken from the impact by increasing the number of movable pulleys on the motor part (n_m) because it affects the impact torque, as shown in (3). All variables used in equations in this paper, including the equations above, are given in Table I.

B. Underactuation Mechanism

An underactuation mechanism simplifies the robot system by using fewer actuators than the number of joints [24]–[27]. This mechanism not only simplifies the system, but also can generate adaptive motions without complex control, when it is used not to apply kinematic constraints, as explained in [25]–[27]. Therefore, this mechanism has been adapted in several wearable

TABLE I
NOTATION USED IN THE ARTICLE

Notation	Definition
n_m	Number of movable pulleys at the motor tendon
ε_M	Gear ratio of the motor
n_e	Number of movable pulleys at the end-effector tendon
R	Radius of the motor spool
τ_M	Motor stall torque
k	Spring constant at the actuation unit
x	Displacement of the slider
w_M	Motor no-load speed
L_t	Total length of the actuator
l_{sta}	Length of the slider
D_{stroke}	Stroke of the actuator
$\mathrm{A_t}$	Actuator total cross-section area
A_{motor}	Initial cross-section area of the motor
a_e	Cross-section area generated by a movable pulley
m_s	Mass of the slider
V_t	Actuator total volume
T_0	Initial tension of the spring
T_M	Tension of the end-effector tendon
μ_{sh}	Friction coefficient between the wire and spring sheath
θ	Curved angle of the spring sheath
μ_{tf}	Friction coefficient between the wire and Teflon tube
μ_b	Friction coefficient between the wire and bearing

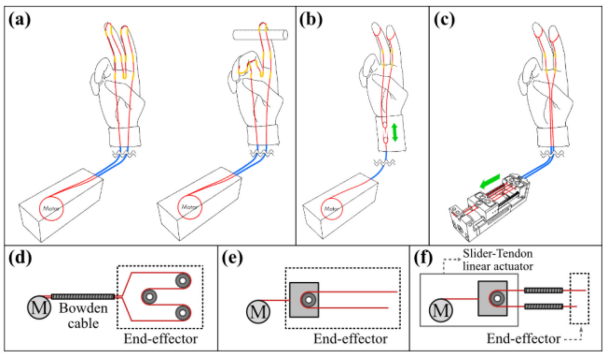

Fig. 4. Methods used to apply tendon-driven under-actuation mechanisms in two links. (a) Shows how the Underactuation mechanism increases the adaptiveness of the robot. Also, (a) and (d) show the underactuation mechanism that uses a fixed pulley. (b) and (e) Show the underactuation mechanism using a movable pulley that is used in the conventional robot. (c) and (f) Show the method of implementing the under-actuation mechanism using the proposed Slider-Tendon linear actuator. The dotted boxes in (d) to (f) mean the end-effector while the other part is located far from the end-effector. Note that the box with the solid line in (f) represents the slider-tendon linear actuator.

robots to make robots adaptable without additional sensors or actuators [20], [21]. We also implemented this mechanism inside the Slider-Tendon linear actuator to make the actuator more suitable for a wearable robot.

In the tendon transmission, a tendon routing that uses a movable pulley is the most common method to realize the underactuation mechanism, as shown in Fig. 4(b) [28]. In this case, the mechanism requires a relatively large volume because of the space that the linear guides need for the pulley to move. To address the size issue, another tendon path using fixed pulleys was proposed, as shown in Fig. 4(a) [20], [29]. In this tendon routing, the tendon is not fixed to the end of the link as is done conventionally; instead, it just passes through the links, and both ends of the wire are fixed to the motor, as shown in Fig. 4(d). Although this method does not require linear space for a movable pulley, the system is not simple because three pulleys are required. Further, the friction is relatively large because it is applied on the wire in all curved paths and is accumulated through the paths. In soft wearable robot research, this accumulated friction becomes a significant problem because conduit-type tendon routers, such as Teflon tubes, are used. Here, the friction at the wire increases exponential to the curved angle, as outlined in the capstan equation [30], [31]. The increased friction reduces several performance measures, including durability, adaptability, efficiency, and control performance. Therefore, a method is required to reduce the friction, while maintaining a compact mechanism size.

This issue can be solved by containing the mechanism in the slider-tendon linear actuator without size increases because the slider in the actuator is already designed to move along the linear guide. By containing the movable pulley in the slider-tendon unit, as shown in Fig. 4(c), the end-effector can be simple compared to a tendon path that uses fixed pulleys. Also, the friction applied to the wire can be dramatically reduced.

C. Fast-Connection Mechanism

A fast-connection is adopted by using the concept of a tendon connector that enables easy separation of the end-effector from the actuator [32]–[34]. The tendon connector is an important component because it maximizes the portability and ease of replacement; this is essential for the actuation techniques used in human assist robots [8]. When the end-effector is detached from the heavy components, the end-effector can be more easily carried. Moreover, a tendon connector allows the wearable part to be easily washed, because the non-waterproof components, such as the actuator and controller, can be easily detached. However, a tendon connector also has a size issue because most of the connectors have been developed using a rigid structure with a linear guide that harms the softness, volume, and weight. The size issue of the tendon connector can be solved by using the slider-tendon linear actuator in the same manner that the actuator solves the problem of the conventional underactuation mechanism, as described in Section II. C. Since the slider in the proposed actuator was originally designed to slide linearly along the actuator, adding the fast-connection mechanism can be established by just making a space for the tendon connector as shown in Fig. 5. It can be found in the green dotted box in Fig. 3.

D. Stroke Amplification Mechanism

Although the slider-tendon linear actuator is designed to be compact, by containing several functions in a single linear unit, the actuator size increases as the required stroke increases. This is because all functions of the slider-tendon unit require linear motion with a longer drive distance than the wire stroke. Additional pulleys are used as movable pulleys in the slider-tendon unit design to reduce the size of the actuator, as shown in

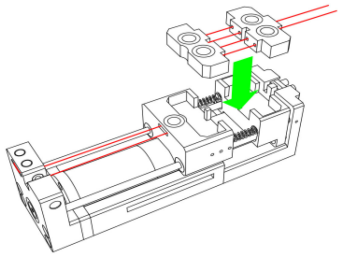

Fig. 5. Schematic showing how the function of fast-connection in the slider-tendon linear actuator works. It includes the function of the fast-connection by separating the end-effector tendon from the slider.

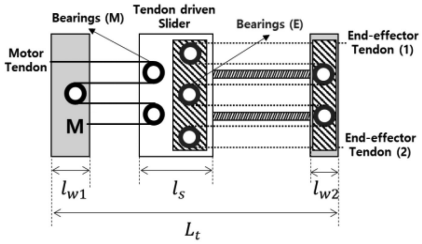

Fig. 6. Schematic showing how the stroke of the Slider-Tendon linear actuator is amplified. Bearings on the end effector side not only allow the slider-tendon linear actuator to have the underactuation mechanism, but also amplify the wire stroke.

Fig. 6. With the given stroke amplification mechanism, the wire stroke (D_{stroke}) can be increased by increasing the number of movable pulleys at the end-effector side, as shown in (5). Here, the l_{sta} refers to the length of actuator components, such as the actuator wall and slider, as defined in (4). From (5), we can infer that the overall actuator length (L_t) can be reduced by using more movable pulleys (n_e). However, an appropriate number of movable pulleys should be used, since the use of the pulley also increases the cross-sectional area of the actuator. The method to induce an appropriate number of movable pulleys is described in more detail in the following section:.

$$l_{\text{sta}} = l_{w1} + l_s + l_{w2} \tag{4}$$

$$2n_e\,(L_t - l_{sta}) = D_{\text{stroke}}. \tag{5}$$

III. Modeling and Mechanical Design

Section III explains the process used to select appropriate components for the slider-tendon linear actuator. For the modeling, we chose a soft wearable robot for a certain application for a specific body part, because the process requires the robot requirements to fix the mechanical components. Our target application was determined to be the Exo-Glove Poly II. The application is shown in Fig. 1; it is a wearable robot designed to assist a hand-paralyzed person in their activities of daily living. The Exo-Glove Poly II has been developed to assist flex motion of the index and middle finger with a single wire using an underactuation mechanism [20].

Since the Exo-Glove Poly II generates motion with a single wire, the actuation requirement can be summarized by the output tension, range of motion (i.e., stroke), and pulling speed of a single wire. This robot requires a 100mm stroke and 80 N tension to assist with grasping in daily life [20]. Further, the robot requirements specify the ability to assist with a grasp in four seconds; therefore, in developing the actuator, the target speed of the tendon should be 25mm/s. Considering the safety factor, the target requirements of the actuator are set as given in Table II. Each component in the slider-tendon linear actuator is determined to increase the efficiency and to minimize the size of the actuator, because the actuator will be carried by a human.

TABLE II
Actuator Requirements for the Exo-Glove-Poly II

Requirement	Value
Tension	100 (N)
Wire stroke	120 (mm)
Pulling and releasing time	4 (sec)

A. Design of the Slider-Tendon Linear Actuator Components

1) Design of a Movable Pulley to Reduce the Size of the Slider-Tendon Linear Actuator: Based on the required stroke of the Exo-Glove Poly II, the actuator size is determined by choosing the number of movable pulleys used in the slider-tendon linear actuator. When the number of movable pulleys is increased, the actuator length can be reduced, as shown in (6); this can be inferred from (5). However, the cross-sectional area of the actuator increases as the number of movable pulleys increases, as shown in (7). We determined the number of movable pulleys as two in our design, because this choice showed the smallest size when using the selected motor. Although the arithmetic-geometric mean of the number of movable pulleys (n_e) enables optimization of the actuator volume, as shown in the (7), the optimal number of pulleys is obtained inductively, rather than deductively. This is because determining the initial size of the actuator is complicated to solve deductively; the size of the actuator varies depending on the design

$$\mathrm{L_t} = l_{\text{sta}} + \frac{D_{\text{stroke}}}{2\mathrm{n_e}} \tag{6}$$

$$\mathrm{A_t} = A_{\text{motor}} + \mathrm{n_e} a_e \tag{7}$$

$$V_t = l_{\text{sta}} A_{\text{motor}} + (D_{\text{stroke}}/2n_e)(n_e a_e + A_{\text{motor}}) + n_e l_{\text{sta}} a_e. \tag{8}$$

After determining the number of pulleys, to show that the movable pulleys are effective to reduce the size, the size of the Slider-Tendon linear actuator (V_{STA}) is compared with that of a ball screw linear actuator (V_{BS}), a slack-enabling actuator (V_{SEA}), and a basic slider-tendon linear actuator that does not use stroke amplification (V_{BSTA}). For equitable comparison, we only estimate the size of the actuation unit because the motor size could differ according to the actuation method. Then, as a function of the actuation stroke (D_{stroke}), the volume of four actuation units are derived as (9)–(12), respectively. Note that the size of the slack-enabling actuator was obtained by referring to the previous research because the slack-enabling actuator is not a commercial product and its size was estimated in the previous

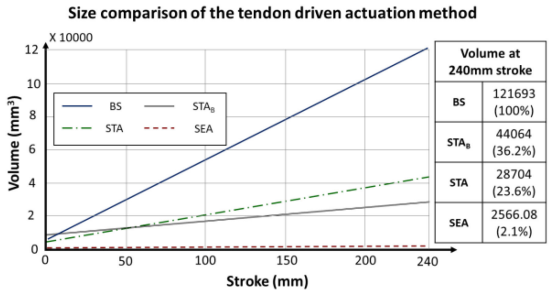

Fig. 7. Size comparison of the tendon-driven actuation unit for a soft wearable robot. The size of the slider-tendon unit is 23.6% of the ball screw. Although the size is reduced, the slider-tendon linear actuator is about 11.2 times bigger than the slack-enabling actuation unit. Values on the right side show the volume of each actuation method when the stroke is 240 mm.

research [17]. Details about the size estimation of other actuation methods are described in the Appendix

$$V_{\mathrm{SEA}} = 264\left(0.018 D_{\mathrm{stroke}} + 5.4\right) \tag{9}$$

$$V_{\mathrm{BSTA}} = 162\left(D_{\mathrm{stroke}} + 32\right) \tag{10}$$

$$V_{\mathrm{STA}} = 312\left(0.25 D_{\mathrm{stroke}} + 32\right) \tag{11}$$

$$V_{\mathrm{BS}} = 481\left(D_{\mathrm{stroke}} + 13\right). \tag{12}$$

Using the equations, the volume of each actuator component is compared, as shown in the graph in Fig. 7. When the required stroke is 240 mm, the size of the Slider-Tendon linear actuator is 23.6% that of the ball screw linear actuator. It is true that the required stroke of the actuator is set to be 120 mm; however, we compared the size at 240 mm so as to not to consider the underactuation, as mentioned above. Although the size of the slider-tendon linear actuator is small, the volume is 10.64 times bigger than the conventional slack-enabling actuation unit.

2) Design of the Spring to Enable a Sufficient Releasing Speed: The other components that affect the actuator performance are the springs used to prevent the wire derailment. When the spring constant is too low, the wire can be derailed from the spool because the slider will move slower than the spool rotation speed. On the other hand, when the spring constant is too high, the actuator efficiency will be reduced as shown in (1). Therefore, we obtained the minimal spring constant required to prevent wire derailment by solving the slider's equation of motion, which is represented as (13). Here, f_{ext} (i.e., the external force) is used for the simplification. The slider position can be solved as shown in (14) with boundary conditions $x(0) = -D_{\mathrm{stroke}}/n_e$ and $x(t_{\mathrm{final}}) = 0$, considering the slider's range of motion

$$m_s\ddot{x} = -kx - \mu_{bs} m_s g + T_0 = -kx + f_{ext} \tag{13}$$

$$x\left(t\right) = \left(-\frac{D_{\mathrm{stroke}}}{n_e} - \frac{f_{\mathrm{ext}}}{k}\right) e^{-\sqrt{\frac{k}{m_s}}t} + \frac{f_{\mathrm{ext}}}{k}. \tag{14}$$

Since the slider should be released within four seconds (based on the robot requirements), the implicit form of the equation to find the desired spring constant (k_{desired}) can be represented as (15). Substituting the actual values of the mechanical properties into the given equation, we can find the spring condition to meet the robot requirements, as shown in (16). Here, the friction coefficient of the bushing (μ_{bs}) is set to 0.01, based on the datasheet; the slider mass (m_s) is directly measured as 30.4 g

$$t_{\mathrm{final}} = \sqrt{\frac{m_s}{k_{\mathrm{desired}}}} \ln\left(1 + \frac{k_{\mathrm{desired}} \times D_{\mathrm{stroke}}}{n_e f_{\mathrm{ext}}}\right) \leq 4 \tag{15}$$

$$k_{\mathrm{desired}} \geq 0.00544. \tag{16}$$

Considering the safety factor to be three, the final spring with a spring constant of 0.02 N/mm was installed in the proposed actuator to result in enough releasing speed.

B. Final Actuator Design with Optimized Components

Using the components chosen as outlined in the previous sections, the final actuator is obtained after selecting the spool size and motor. First, the power of the motor is selected by considering the requirements for tension and wire speed. In this article, an 8.5 W motor (Faulhaber, 2224SR, ∅22mm, length 24 mm) is selected to achieve the required tension and speed. The motor length is 58.7mm when the gearbox is attached. Second, the gear ratio and spool size are determined because these variables are all related to the force-speed relationship. We first determined the diameter of the motor spool prior to the gear ratio decision because the spool size is related to the impact torque applied to the motor and the reliability of the wire. When the spool size is reduced, the external impact force applied to the wire is transmitted to the motor with a small torque. Therefore, it can be prevented from damaging the motor when an impact force is applied to the wire. However, if the size of the spool is too small, it will promote wear of the wire, thus, the spool size must be kept in the proper size to prevent wear. The size of the motor spool is determined to be 5 mm in diameter, so as to not bend the wire; this was determined using the equation defined in previous research [35], [36]. Then, the tension and speed of the end-effector tendon can be calculated as 3.39 N and 2146.75 mm/s, respectively. Note that these values are calculated for a situation in which an underactuation mechanism is used. Therefore, the gear ratio should be larger than 29.48 to make the wire tension larger than 100 N, while the gear ratio should be also smaller than 71.56 to make wire-speed faster than 30 mm/s. With the given condition for the gear ratio, a gearbox (Faulhaber, 22E) with a gear ratio of 69:1 is used to satisfy the actuator requirements. Considering the gear efficiency of the selected gearbox as 0.69, the final wire tension, pulling speed, and stroke are 161.49 N, 31.11 mm/s, and 124 mm, respectively. Therefore, we can conclude that the final actuator performance satisfies the robot requirements, which are given in Table II.

The slider-tendon linear actuator has two movable pulleys to minimize the volume and the internal spring is used to have a spring constant of 0.02 N/mm. The final size of the actuator is 35 mm height, 112.9 mm length, and 34 mm width. Also, the total actuator weight is 162.2 g, of which 66.3 g is the weight of the motor. The actuator size is relatively large compared to the estimation in the previous section because additional components are included in the actuator. Specifically, a single loadcell (LSB200, Futek, USA) is included for tension control. The loadcell is added because the gear ratio of the selected motor is high; thus, the friction at the gearbox of the motor cannot be ignored. Here, admittance control is used to control

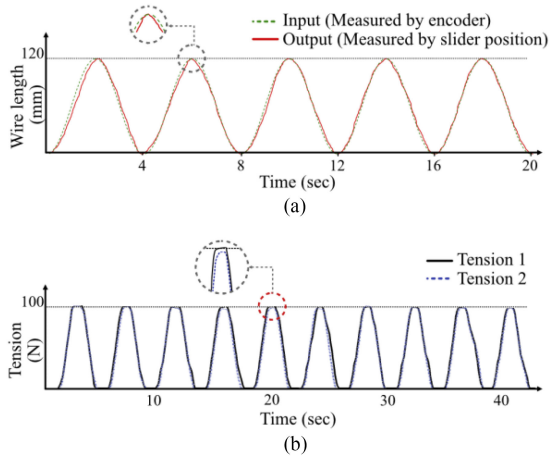

Fig. 8. (a) Actuator performance in position and (b) force domain. The actuator pulls wire 120 mm in two seconds in a no-load condition. The rms error between the estimated and real slider position is 3.61%. The blue dotted line in figure (a) is the pulled length calculated by the encoder and the black solid line is the pulled length of the wire calculated by the slider position. Figure (b) shows that the tension of the wire reaches to 100 N and the tension applied on the two wires is similar.

the tension of the tendon. Details about the tension control used in the proposed actuator are described in [37]. Also, the space to fix the Bowden cable is included in the final actuator. All actuation characteristics are verified in the next section.

IV. Simulation and Performance

In this section, we show whether or not the final actuator design satisfies the robot requirements through both simulation and experiment. First, experiments that measure the tension and speed of the wire are conducted. Next, a second experiment that shows the effectiveness of the under-actuation mechanism is conducted with a simulation that derives the tension distribution.

A. Validation of the Actuator Speed

The slider-tendon linear actuator contains springs that have a spring constant of 0.02 N/mm. First, we measured the speed of the slider to check whether the selected spring works well. This is because the wire speed is related to the slider speed, rather than the rotational speed of the motor. To measure the speed of the slider without affecting the actuation, captured video is analyzed by MATLAB (Mathworks, Natick, MA, USA). The real position of the slider and estimated position using the motor encoder data are compared, as shown in Fig. 8(a). Since the tension increases after contact in our application, this experiment was conducted in a no-load condition. The tension begins to increase only at the last moment when it contacts the object; thus, the experiment under a no-load condition does not differ from the actual situation. The blue dotted line in the graph shows the estimated position of the slider calculated with the encoder data and the black solid line means the measured position of the slider using video analysis. The RMS error between the estimated and real position is 3.61%. It is important to note that, the wire length at the y-axis of the Fig. 8(a) is total pulled length of the tendon. This implys that the actual speed of the tendon could be 30 mm/s (half of the result shown in Fig. 8), when the under-actuation mechanism is considered. However, this does not matter as it satisfies the requirement in Table II.

After the speed experiment, wire tension is also measured using the loadcell. Since the slider-tendon unit contains an underactuation mechanism, the tension of both ends of the wire is measured. The force properties results are depicted in Fig. 8(b). As a result, the tension at each wire sufficiently reaches the requirements of the application, and the tension difference between the two wires is small. In this experiment, the root mean value of the tension difference is 0.78 N.

B. Simulation and Validation of the Underactuation Mechanism

In Section II, we explained two underactuated tendon routings (e.g., tendon routing using the movable pulley and routing using the fixed pulleys), as depicted in Fig. 4. Although routings are designed to have the same function (i.e., function to apply the underactuaion mechanism on the two-link system), the tension distribution shows a difference due to the difference of tendon path and the routing components (pulley, conduit, bearing, etc.). The tension distribution of two different tendon routings can be obtained by figuring out the friction applied on the tendon. The friction applied on the tendon can be simply modeled using the capstan equation [30], [31]. In this equation, the friction applied on the wire is defined as (35), where μ is the Coulomb friction coefficient, T is tension of the tendon, and θ is the angle of the curve at the tendon routing. Note that the Coulomb friction model is well used in the capstan equation among various friction models [38]. In capstan equation that uses the Coulomb friction, the tendon friction depends on how the wire is routed. When non-rotating components (i.e., a nonrotating router) such as conduits are used, relative movement between the wire and the routing component induces the kinetic friction. On the other hand, in a case that uses rotating components (i.e., a rotating router) such as a bearing or spool, rolling resistance is applied. In this article, for the nonrotating router, the Coulomb friction coefficient is defined as 0.05, while for the rotating router, the friction coefficient is defined as 0.001. This is because the Exo-Glove Polly II uses Teflon tubes as non-rotating routers (i.e., conduits) and the slider-tendon linear actuator uses bearings as rotating routers (i.e., pulleys) [21]

$$f = T\left(1 - e^{-\mu\theta}\right). \tag{35}$$

By extending the content about friction to the whole tendon routing, the overall tension distribution can be derived by considering the direction of the wire movement, friction coefficient, and the elongation of the wire. To do so, we simplified the tendon routing in the finger to the routing shown in Fig. 9. In this schematic, the friction was derived by dividing the tendon into several segments. In Fig. 9(a), the wire is divided into six segments in the tendon routing; two segments at the actuator side (a, b), and four segments at the end-effector side (1 to 4). The upper block in the figure refers to link A (finger A in the wearable robot application) and is assumed to have contact with the external environment, while link B (finger B in the wearable robot application) that is depicted as the lower block is assumed to move freely.

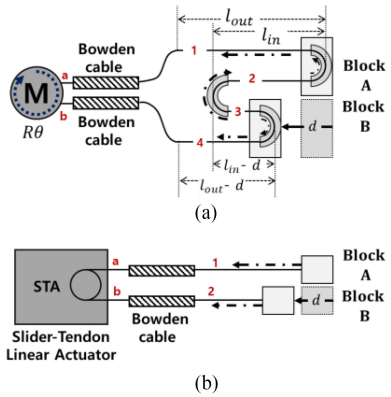

Fig. 9. Schematic of the tendon routing to analyze the tension distribution. For simplification, fingers are assumed as a block that moves linearly. (a) Underactuated tendon path using fixed pulleys. (b) Underactuated tendon path using a movable pulley.

In the tendon routing with fixed pulleys [see Fig. 9(a)], the wire at segment a and b will be wound around the spool amount of $R\theta$(R means spool radius), respectively, when the spool rotates an amount of θ. As block A does not move, the length of segments *1* and *2* does not change, while the lengths of segments 3 and 4 decrease in the amount of d when block B moves an amount of d. Then, it is obvious that the traveling length of the lower block (d) is equal to the wound length of the spool ($R\theta$), which is described as (37). The notation used in this equation is depicted in Fig. 9(a)

$$2(l_{\text{out}} + l_{\text{in}}) - 2R\theta = 2(l_{\text{out}} + l_{\text{in}} - d) \tag{36}$$

$$R\theta = d. \tag{37}$$

In this tendon routing, the wire at segment 3 will move to segment a by passing through segments 2 and 1. This is because the lengths of segments 2 and 1 do not change, while the length of segment 3 is reduced. On the other hand, the wire at segment *4* directly moves to segment b. The aspects of the movement of the end-effector wire when the motor pulls the wire can be depicted as the arrow in Fig. 9(a). In this case, one unusual aspect is presented: there is no movement in the wire between segments 3 and 4. Here, we used an additional assumption that the wire elongates when the tension increases. With this assumption, it is possible to consider the movement between these segments. This is important because the static friction is difficult to estimate. As a result, we can envision that the elongated wire in segment 3 moves to segment 4. Given information about the direction of wire movement, total tension distribution is obtained as given in Table III. In addition, we defined the concept of the transmission ratio, a ratio of the pulled length of the wire by the actuator to the moving distance of the link, to obtain the relation between the motor torque and the fingertip force using the virtual work principle. The routing system with fixed pulleys has a transmission ratio of 1:1 because the wound length of the wire is equal to the traveling distance of the lower block, as (36) shows.

When the underactuation is implemented with the movable pulley, as in Fig. 9(b), the wire can be divided into four segments;

TABLE III
TENSION DISTRIBUTION OF THE TENDON ROUTING WITH FIXED PULLEYS

Tension relationship		Tension distribution	
$T_M = T_a + T_b$	(17)	$T_1 = G_\mu T_M e^{-\mu_{sh}\theta}$	(23)
$T_1 = T_a e^{-\mu_{sh}\theta}$	(18)	$T_2 = G_\mu T_M e^{-\mu_{sh}\theta-\mu_{tf}\pi}$	(24)
$T_4 = T_b e^{-\mu_{sh}\theta}$	(19)	$T_3 = G_\mu T_M e^{-\mu_{sh}\theta-2\mu_{tf}\pi}$	(25)
$T_2 = T_1 e^{-\mu_{tf}\pi}$	(20)	$T_4 = G_\mu T_M e^{-\mu_{sh}\theta-\mu_{tf}\pi}$	(26)
$T_3 = T_2 e^{-\mu_{tf}\pi}$	(21)	$G_\mu = \frac{1}{1+exp(-\mu_{tf}\pi)}$	(27)
$T_3 = T_4 e^{-\mu_{tf}\pi}$	(22)		

TABLE IV
TENSION DISTRIBUTION OF TENDON ROUTING WITH A MOVABLE PULLEY

Tension relationship		Tension distribution	
$T_M = T_a + T_b$	(28)	$T_1 = G_{\mu_b} T_M e^{-\mu_{sh}\theta}$	(32)
$T_b = T_a e^{-\mu_b\pi}$	(29)	$T_4 = G_{\mu_b} T_M e^{-\mu_{sh}\theta-\mu_b\pi}$	(33)
$T_1 = T_a e^{-\mu_{sh}\theta}$	(30)	$G_{\mu_b} = \frac{1}{1+exp(-\mu_b\pi)}$	(34)
$T_4 = T_b e^{-\mu_{sh}\theta}$	(31)		

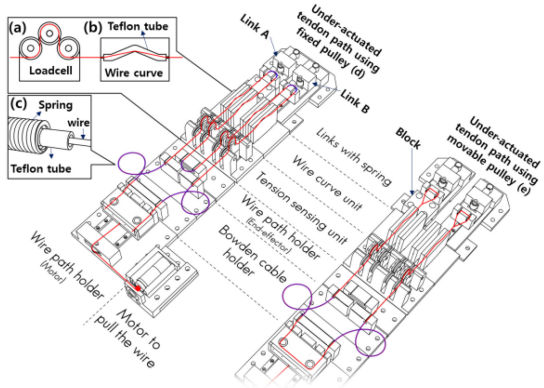

Fig. 10. Experimental setup to measure the tension distribution of the tendon routing. (a) Method to measure the tension with curved tendon routing. The wire curve unit in (b) intentionally makes the wire bend. (c) Schematic of Bowden cable. By changing the tendon routing, tension distribution of two tendon routings is measured.

two segments in the motor part (a and b) and two segments in the end-effector part (1 and 2). Here, the wire in segment 2 moves to segment a after passing segment b. The wire at segment 1 does not move because link A does not have movement. However, when we assume elongation of the wire, the wire at segment 1 also moves to segment a. In this case, the transmission ratio is 2:1 because the link moves twice the length of the wire wound by the spool. The tension relationship between each segment and the final tension distribution is derived as given in Table IV.

Experiments to validate the underactuation performance are conducted as shown in Fig. 10. To create a situation in which the link moves slowly with increasing wire tension, springs are connected to each link. To make the situation of contact, an additional block is installed in front of the link. Four load cells are used to measure the segmental tension of a single wire divided into segments. Fig. 10(d) and (e) shows the tendon paths of under-actuation that use conduits and movable pulleys, respectively.

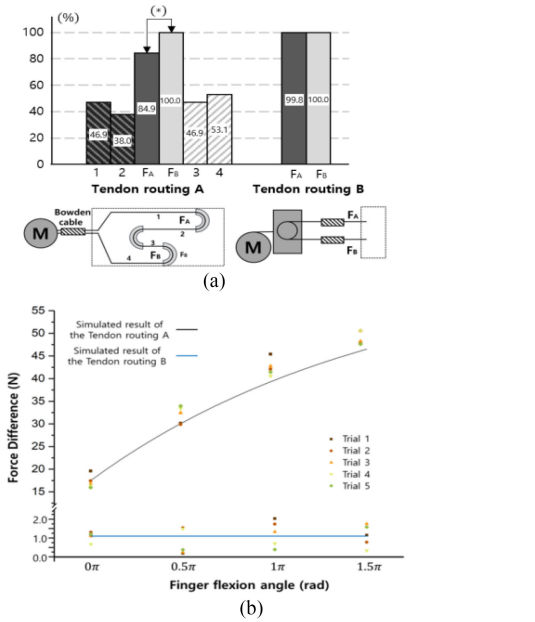

Fig. 11. (a) Experimental and simulated results of the force difference that is applied to the finger (a). (∗) means that there is a significant difference between the two results. (b) How the force differences varies when the finger flexion occurs. Since the ratio of the force applied to the two fingers is important in the under-actuation mechanism, both graphs are represented by converting all values as a percentage of the force exerted on one finger (F_B).

To measure the tension, a tension meter is designed, as shown in Fig. 10(a), by referring to the conventional method of measuring the tension. Experimental equipment includes a wire curve unit to reflect the change in the wire path caused by finger bending; the curve unit is designed as shown in Fig. 10(b). Inside the curve unit, the Teflon tube is installed at a certain bending angle. The finger bending angle can be considered by replacing the unit that curves at different angles. The tension meter is located after the wire curve unit because the measurement of how much force the wire transfers to each finger is a goal of the experiment.

Using the experiment setup introduced above, the tension distribution of the tendon routing using fixed pulleys and the routing using movable pulleys are each obtained, as shown in Fig. 11(a). F_A and F_B each mean the force applied on two fingers; the 1 to 4 notations in the tendon routing using fixed pulleys refer to the tension at the wire segment that is introduced in Fig. 9. In this experiment, we found that the difference between F_A and F_B is 15.1N when the fixed pulley is used, while the difference between the two fingers is only 0.2 N when the movable pulley is used. Here, the experiment was conducted until the sum of the forces applied to finger B reached 100 N.

The experiment described above was conducted when the curve angle of the wire curve unit was 0 rad, which means that the finger is fully extended. The experimental results of measuring the difference in the force of the fingers according to the variation of the bent angle are shown in Fig. 11(b). The routing using fixed pulleys shows that the difference in force applied to the two fingers increases as the angle of bending of the finger increases. On the other hand, in the case of underactuation using a movable pulley, it can be found that the difference in the force does not cause a significant change as the bending angle of the finger changes.

V. Conclusion

A tendon transmission has been used in the soft wearable robot because of its advantages, which make the end effector more compact, light, and simple. However, the tendon transmission requires special care so as to not induce high friction and such that the wire does not become tangled around the spool. To address these issues, researchers have applied additional functions to the tendon transmission, such as a pretension mechanism or a slack-enabling mechanism. Other techniques, such as using an underactuation mechanism or a fast-connection, have also been proposed to simplify and minimize the end-effector. In this article, we proposed a linear actuator that is driven with a tendon, rather than a ball screw to reduce the actuator size. Furthermore, a design methodology to contain several mechanisms is applied in the actuator design. The proposed actuator contains an underactuation mechanism for robot adaptability, a fast-connection mechanism for portability, and a stroke amplification mechanism for size minimization. By doing so, it was possible to simplify the end-effector, and also to improve the performance of the robot. Performance is improved due to the slider-tendon's easy-to-use mechanical components; reduced mechanical components in the end-effector also result in increased wearability, simplicity, and compactness.

It should be noted that the durability of the proposed actuator may be less than that of a conventional ball screw transmission. However, although durability is of course important, the Slider-Tendon's durability will be sufficient if its durability is higher than the durability of the Bowden cable. Since the wire slips at the Bowden cable, the durability of the actuator is higher than that of the Bowden cable [31], [39], [40]. Because the Slider-Tendon linear actuator offers advantages in size, we can conclude that the slider-tendon linear actuator is more suitable for tendon-driven wearable robots that use a bowden cable. also, other advantages of ball screws, such as back-drivability and accuracy are not meaningful in a system using a Bowden cable because the friction at the Bowden cable degrades these advantages.

The proposed actuation method also has additional minor advantages that are not explained elsewhere in this article. First, the actuator is inexpensive because it consists of only two bushings and two springs. Second, the actuator can be easily customized to meet the requirements of a particular robot by changing the motor spool size, the number of pulleys, and the gear ratio. In addition, the slider-tendon linear actuator can be a good solution for high-impact situations by reducing the radius of the spool and increasing the number of pulleys on the motor side. By changing these parameters, damage to the motor from a large impact can be avoided.

The size of the proposed actuator is 23.6% of the ball screw actuator size and 10.64 times bigger than that of the slack-enabling mechanism. However, the durability of

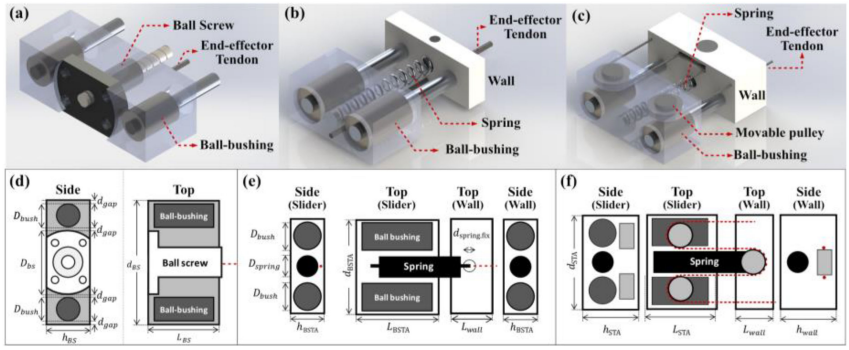

Fig. 12. Schematic of each actuation method for the size comparison (a) and (d) show a ball screw linear actuator (BS), (b) and (e) show a basic slider-tendon linear actuator, and (c) and (f) show a slider-tendon linear actuator with stroke amplification. Figure (a)–(c) show the overall view of each actuation methods and the figures (d)–(f) show the schematic view to derive the estimated size of the actuation methods. The red dotted lines in figures (d)–(f) are the end-effector tendon of the robot system.

the slack-enabling actuator is not sufficient for many practical applications, since it uses friction and slips for derail prevention. In practical use, the reliability of the slack-enabling actuator was even less than that of the Bowden cable. Also, the slack-enabling actuator does not have a space for the linear motion, which makes it difficult for it to adopt additional functions, such as fast-connection and underactuation.

The slider-tendon linear actuator also has the potential to contain other components used in other research about tendon transmissions with rotary motors [22], [23]. First, the actuator can increase the peak tension by using a compliant material. By adding a compliant component that accumulates spring energy in the unwinding process and emits energy in the winding process, we can increase the maximum tension without using a high-torque motor. Also, research of adding an extra spool in parallel to the existing spool can be pursued. In this design, the actuator can pull two wires, even using a single motor. Therefore, we can make the actuator apply bidirectional force as a dual slack-enabling actuator, as shown in previous research [17]. Other research related to changing the radius of the motor spool can also be used in the slider-tendon linear actuator. This article uses a motor spool as a transmission. It generates high tension by decreasing the radius of the motor spool and generates high speed by increasing the radius of the spool [41].

The proposed actuator will require additional research about the type of wire. The wire used in the proposed actuator is Dyneema because this wire has high yield strength. However, the wire used in the article has high hysteresis, which is not preferred in force control. Therefore, the best wire to be used in the actuator should be chosen based on future work. Additional research should also be performed to increase the performance of the tendon transmission. Friction and the wear of the wire is one of the main disadvantages that leads many researchers to hesitate to use a tendon transmission. In future work, a wear-monitoring system can be proposed for the slider-tendon linear actuator. By measuring and comparing the tension at the end-effector and on the actuator side, the system can observe the tendon wear. As a long-term goal, we are eager to make the tendon transmission a compact, safe, and reliable transmission to be used in human assist robots by adding more functions to the slider-tendon linear actuator proposed here.

APPENDIX

This section provides a detailed explanation about how we derive the volume of several transmissions to pull the tendon, as introduced in Section III-A. Here, the volume of the ball screw transmission, slider-tendon transmission with stroke amplification, and slider-tendon transmission without stroke amplification are derived. Note that the volume of the slack-enabling mechanism is not estimated because this was estimated in previous research, as explained in the main text [17]. The size estimation begins by defining the several assumptions, as outlined later.

First, we only estimate the size of the actuation unit; the motor size is excluded to allow more equitable comparison. Second, each size of the actuation method is compared by calculating the volume of the smallest cube that surrounds the actuation unit; each volume is calculated by multiplying the cross-sectional area and height. Third, all the gap between each mechanical part (d_{gap} in Fig. 12) is set as 1mm. Fourth, estimation is carried out by considering the larger part when several parts are placed in parallel. For example, the length of the actuation unit with a ball screw (L_{BS}) is determined by the length of the longer part among the ball bushing and ball screw because the ball bushing and the ball screw are placed in a row, as shown in Fig. 12(a). The function *max* is used to express this situation as shown in (41). Lastly, the size of the slider-tendon linear actuator is estimated without considering its ability to include the under-actuation mechanism or the fast-connection; this enables fair comparison because the other actuation unit also does not contain these functions.

In the size estimation of the actuation unit with the ball screw, the volume is calculated using the smallest ball screw among commercially available products because the ball screw is a commercial product; this is named “MDK-0401-3” [42], [43]. The schematic of the actuation unit with the ball screw is shown in Fig. 12(a). Since the given ball screw requires an additional linear ball bushing for the linear motion, the size of the actuation unit with the ball screw is estimated by including the space needed for the bushing, which is depicted in dark gray in Fig. 12(a). Two bushings are used because the flange of the ball screw must be designed to have force equilibrium to minimize friction. For a fair comparison, the Slider-Tendon design also

TABLE V
PARAMETERS FOR ACTUATOR SIZE ESTIMATION

Design parameter	Value (mm)
Gap between mechanical components (d_{gap})	1
Diameter of bushing (D_{bush})	7
Length of bushing (L_{bush})	10
Diameter of flange (D_{bs})	19
Width of flange (T_{bs})	13
Length of flange (L_{bs})	13
Diameter of bearing ($D_{bearing}$)	8
Height of bearing ($h_{bearing}$)	2
Diameter of spring (D_{spring})	3
Length of spring (l_{spring})	30
Diameter of bolt to fix the spring ($d_{spring.fix}$)	2

includes two linear ball-bushings of the same size used in the ball screw size estimation. Since the ball screw has different lengths in horizontal ($T_{\rm bs}$) and vertical directions (D_{bs}), the size of the ball screw is estimated by using the smaller value among $A_{\rm BS}^{\rm ver}$ in (38) and $A_{\rm BS}^{\rm hor}$ in (39), as shown in (40). Actuator size can be estimated using (42), with the design parameters given in Table V

$$A_{\rm BS}^{\rm ver} = h_{\rm bs}\left(D_{\rm bs} + 2D_{\rm bush} + 4d_{\rm gap}\right) \tag{38}$$
$$A_{\rm BS}^{\rm hor} = D_{\rm bs}\left(h_{\rm bs} + 2D_{\rm bush} + 4d_{\rm gap}\right) \tag{39}$$
$$A_{\rm BS} = \min\left(A_{\rm BS}^{\rm ver},\ A_{\rm BS}^{\rm hor}\right) \tag{40}$$
$$L_{\rm BS} = \max\left(L_{\rm bs}, L_{\rm bush}\right) + 2d_{\rm gap} \tag{41}$$
$$V_{\rm BS} = A_{\rm BS} \times \left(D_{\rm stroke} + L_{\rm BS}\right) = 481\left(D_{\rm stroke} + 13\right). \tag{42}$$

For the case of the basic slider-tendon linear actuator (BSTA), which is a slider-tendon linear actuator that does not use stroke amplification, the size of the actuation unit is derived using the schematic shown in Fig. 12(b). The size of the BSTA is estimated as follows. In the BSTA size estimation, $L_{\rm BSTA}^{\rm final}$ is relatively complicated since the space to fix the spring should be considered. Since the spring is fixed both at the slider and at the wall, the $L_{\rm wall}$ and $L_{\rm BSTA}$ must be considered in the estimation, as shown in (46) and (47). However, if the length of the spring is longer than the sum of the length of the wall and the length of the slider, the length of the spring will affect the volume; the length of the entire actuation unit is expressed as shown in (46)

$$V_{\rm BSTA} = \left(L_{\rm BSTA}^{\rm final} + D_{\rm stroke}\right) \times d_{\rm BSTA} \times h_{\rm BSTA} \tag{43}$$
$$h_{\rm BSTA} = \left(2d_{\rm gap} + \max\left(D_{\rm bush}, D_{\rm spring}\right)\right) \tag{44}$$
$$d_{\rm BSTA} = \left(D_{\rm spring} + 2D_{\rm bush} + 4d_{\rm gap}\right) \tag{45}$$
$$L_{\rm BSTA}^{\rm final} = \max\left(L_{\rm wall} + L_{\rm BSTA}, L_{\rm spring} + 2d_{\rm gap}\right) \tag{46}$$
$$L_{\rm BSTA} = 2d_{gap} + L_{\rm bush} \tag{47}$$
$$L_{\rm wall} = 2d_{\rm gap} + d_{\rm spring.fix.} \tag{48}$$

To show the effect of the additional movable pulley, we also obtained the size of the actuator that arises from using a slider-tendon linear actuator with two movable pulleys (STA), as shown in Fig. 3. The size of the slider-tendon unit is estimated as shown in (49) and (50). Since two movable pulleys are used, 0.25 is multiplied by the stroke of the wire in the final volume estimation

$$V_{\rm STA} = \left(L_{\rm STA}^{\rm final} + 0.25D_{\rm stroke}\right) \times d_{\rm STA} \times h_{\rm STA} \tag{49}$$
$$d_{\rm STA} = \max\left(3D_{\rm bearing} + 2d_{\rm gap}, 2D_{\rm bush} + D_{spring} + 4d_{\rm gap}\right) \tag{50}$$
$$h_{STA} = \left(3d_{\rm gap} + \max\left(D_{\rm bush}, D_{\rm spring}\right) + h_{\rm bearing}\right) \tag{51}$$
$$L_{\rm STA}^{\rm final} = \max\left(L_{\rm wall} + L_{\rm STA}, L_{\rm spring} + 2d_{\rm gap}\right) \tag{52}$$
$$L_{\rm wall} = \max\left(D_{\rm bearing}, d_{\rm sp\_fix}\right) + 2d_{\rm gap} \tag{53}$$
$$L_{\rm STA} = 2d_{\rm gap} + \max\left(L_{\rm bush}, D_{\rm bearing}\right). \tag{53}$$

With the actual size of the component, the size of the slider-tendon unit and BSTA can be estimated. One note is that a single spring was included in the slider-tendon unit size estimation; however, two springs are used in the actual design, as shown in the Fig. 3. This is because it is more compact to attach springs to both sides than to connect a spring at the center when the motor or tendon connector is considered. Since the assumption in this estimation is to ignore the effect of the tendon connector or motor, the size is estimated using a single spring.

REFERENCES

[1] W. T. Townsend, "The effect of transmission design on force controlled manipulator performance," Ph.D. dissertation, Dept. Mech. Eng., Massachusetts Inst. Technol., Cambridge, MA , USA, 1988.

[2] D. Ogane, K. Hyodo, and H. Kobayashi, "Mechanism and control of a 7 DOF tendon-driven robotic arm with NST," *J. Robot. Soc. Jpn.*, vol. 14, no. 8, pp. 1152–1159, 1996.

[3] M. Xiloyannis, L. Cappello, D. B. Khanh, S. C. Yen, and L. Masia, "Modelling and design of a synergy-based actuator for a tendon-driven soft robotic glove," in *Proc. IEEE RAS EMBS Int. Conf. Biomed. Robot. Biomechatron.*, 2016, pp. 1213–1219.

[4] J. Guo *et al.*, "A soft robotic exo-sheath using fabric EMG sensing for hand rehabilitation and assistance," in *Proc. IEEE Int. Conf. Soft Robot. RoboSoft*, 2018, pp. 497–503.

[5] M. Xiloyannis, L. Cappello, K. D. Binh, C. W. Antuvan, and L. Masia, "Preliminary design and control of a soft exosuit for assisting elbow movements and hand grasping in activities of daily living," *J. Rehabil. Assist. Technol. Eng.*, vol. 4, pp. 1–15, 2017.

[6] F. A. Panizzolo *et al.*, "A biologically-inspired multi-joint soft exosuit that can reduce the energy cost of loaded walking," *J. Neuroeng. Rehabil.*, vol. 13, no. 1, pp. 1–14, 2016.

[7] D. Park and K. J. Cho, "Development and evaluation of a soft wearable weight support device for reducing muscle fatigue on shoulder," *PLoS One*, vol. 12, no. 3, pp. 1–24, 2017.

[8] A. J. Veale and S. Q. Xie, "Towards compliant and wearable robotic orthoses: A review of current and emerging actuator technologies," *Med. Eng. Phys.*, vol. 38, no. 4, pp. 317–325, 2016.

[9] K. Y. Wu, Y. Y. Su, Y. L. Yu, C. H. Lin, and C. C. Lan, "A 5-Degrees-of-Freedom lightweight elbow-wrist exoskeleton for forearm fine-motion rehabilitation," *IEEE/ASME Trans. Mechatronics*, vol. 24, no. 6, pp. 2684–2695, Dec. 2019.

[10] M. Lee *et al.*, "A compact ankle exoskeleton with a multi-axis parallel linkage mechanism," *IEEE/ASME Trans. Mechatronics*, early access, Jul. 10, 2020, doi: 10.1109/TMECH.2020.3008372.

[11] E. Trigili *et al.*, "Design and experimental characterization of a shoulder-elbow exoskeleton with compliant joints for post-stroke rehabilitation," *IEEE/ASME Trans. Mechatronics*, vol. 24, no. 4, pp. 1485–1496, Aug. 2019.

[12] Y. Ding, I. Galiana, A. Asbeck, B. Quinlivan, S. M. M. De Rossi, and C. Walsh, "Multi-joint actuation platform for lower extremity soft exosuits," in *Proc. IEEE Int. Conf. Robot. Autom.*, 2014, pp. 1327–1334.

[13] X. Hu, A. Chen, Y. Luo, C. Zhang, and E. Zhang, "Steerable catheters for minimally invasive surgery: A review and future directions," *Comput. Assist. Surg.*, vol. 23, no. 1, pp. 21–41, 2018.

[14] A. T. Asbeck, K. Schmidt, I. Galiana, D. Wagner, and C. J. Walsh, "Multi-joint soft exosuit for gait assistance," in *Proc. IEEE Int. Conf. Robot. Autom.*, 2015, vol. 2015, pp. 6197–6204.
[15] Y. Mao and S. K. Agrawal, "Design of a cable-driven arm exoskeleton (CAREX) for neural rehabilitation," *IEEE Trans. Robot.*, vol. 28, no. 4, pp. 922–931, Aug. 2012.
[16] V. Chernyak *et al.*, "The design and realization of a high mobility biomimetic quadrupedal robot," in *Proc. 8th IEEE/ASME Int. Conf. Mechatronic Embed. Syst. Appl.*, 2012, pp. 93–98.
[17] H. In, U. Jeong, H. Lee, and K. J. Cho, "A novel slack-enabling tendon drive that improves efficiency, size, and safety in soft wearable robots," *IEEE/ASME Trans. Mechatronics*, vol. 22, no. 1, pp. 59–70, Feb. 2017.
[18] M. Grebenstein *et al.*, "The hand of the DLR hand arm system: Designed for interaction," *Int. J. Rob. Res.*, vol. 31, no. 13, pp. 1531–1555, 2012.
[19] L. Cao *et al.*, "Sewing up the wounds: A robotic suturing system for flexible endoscopy," *IEEE Robot. Autom. Mag.*, vol. 27, no. 3, pp. 45–54, Sep. 2020.
[20] H. In, B. B. Kang, M. Sin, and K. Cho, "Exo-Glove: A wearable robot for the hand with a soft," *IEEE Robot. Autom. Mag.*, vol. 22, no. 1, pp. 97–105, Mar. 2015.
[21] B. B. Kang, H. Choi, H. Lee, and K. J. Cho, "Exo-Glove poly II: A polymer-based soft wearable robot for the hand with a tendon-driven actuation system," *Soft Robot,* vol. 6, no. 2, pp. 214–227, 2019.
[22] D. J. Hyun, H. S. Lim, S. I. Park, and S. Nam, "Singular wire-driven series elastic actuation with force control for a waist assistive exoskeleton, H-WEXv2," *IEEE/ASME Trans. Mechatronics*, vol. 25, no. 2, pp. 1026–1035, Apr. 2020.
[23] Y. Jung and J. Bae, "Torque control of a series elastic Tendon-sheath actuation mechanism," *IEEE/ASME Trans. Mechatronics*, vol. 25, no. 6, pp. 2915–2926, Dec. 2020.
[24] F. Wang, Z. Qian, Z. Yan, C. Yuan, and W. Zhang, "A novel resilient robot: Kinematic analysis and experimentation," *IEEE Access*, vol. 8, pp. 2885–2892, 2020.
[25] A. M. Dollar and R. D. Howe, "The highly adaptive SDM hand: Design and performance evaluation," *Int. J. Rob. Res.*, vol. 29, no. 5, pp. 585–597, 2010.
[26] Z. Jingdong, J. Li, S. Shicai, C. Hegao, L. Hong, and H. Gerd, "A five-fingered underactuated prosthetic hand system," in *Proc. IEEE Int. Conf. Mechatronics Autom.*, vol. 2006, 2006, pp. 1453–1458.
[27] T. Lalibert, G. Cl´ement, and F. Pelletier, "An anthropomorphic underactuated robotic hand with 15 dofs and a single actuator," in *Proc. IEEE Int. Conf. Robot. Autom.*, 2008, pp. 749–754.
[28] L. Birglen and C. M. Gosselin, "Force analysis of connected differential mechanisms: Application to grasping," *Int. J. Rob. Res.*, vol. 25, no. 10, pp. 1033–1046, 2006.
[29] M. G. Catalano, G. Grioli, E. Farnioli, A. Serio, C. Piazza, and A. Bicchi, "Adaptive synergies for the design and control of the Pisa/IIT softhand," *Int. J. Rob. Res.*, vol. 33, no. 5, pp. 768–782, 2014.
[30] X. Li, A. M. H. Tiong, L. Cao, W. Lai, P. T. Phan, and S. J. Phee, "Deep learning for haptic feedback of flexible endoscopic robot without prior knowledge on sheath configuration," *Int. J. Mech. Sci.*, vol. 163, 2019, Art. no. 105129.
[31] U. Jeong, K. Kim, S. H. Kim, H. Choi, B. D. Youn, and K. J. Cho, "Reliability analysis of a tendon-driven actuation for soft robots," *Int. J. Rob. Res.*, pp. 1–18, 2020.
[32] J. Ingvast and J. Bolin, U.S. Patent 8 814 460, Aug. 2014.
[33] M. Nilsson, J. Ingvast, J. Wikander, and H. Von Holst, "The soft extra muscle system for improving the grasping capability in neurological rehabilitation," in *Proc. IEEE-EMBS Conf. Biomed. Eng. Sci.*, 2012, pp. 412–417.
[34] D. H. Kim and H. S. Park, "Cable actuated dexterous (CADEX) glove for effective rehabilitation of the hand for patients with neurological diseases," in *Proc. IEEE Int. Conf. Intell. Robot. Syst.*, 2018, pp. 2305–2310.
[35] A. Horigome, G. Endo, A. Takata, and Y. Wakabayashi, "Development of new terminal fixation method for synthetic fiber rope," *IEEE Robot. Autom. Lett.*, vol. 3, no. 4, pp. 4321–4328, Oct. 2018.
[36] A. Horigome and G. Endo, "Basic study for drive mechanism with synthetic fiber rope-investigation of strength reduction by bending and terminal fixation method," *Adv. Robot.*, vol. 30, no. 3, pp. 206–217, 2016.
[37] B. Kim, J. Ryu, and K. Cho, "Joint angle estimation of a Tendon-driven soft wearable robot through a tension and stroke measurement," *Sensors*, vol. 20, pp. 1–20, 2020.
[38] Y. F. Liu, J. Li, Z. M. Zhang, X. H. Hu, and W. J. Zhang, "Experimental comparison of five friction models on the same test-bed of the micro stick-slip motion system," *Mech. Sci.*, vol. 6, no. 1, pp. 15–28, 2015.
[39] M. Z. Huq and J. P. Celis, "Expressing wear rate in sliding contacts based on dissipated energy," *Wear*, vol. 252, no. 5–6, pp. 375–383, 2002.
[40] A. Cruzado, M. A. Urchegui, and X. Gómez, "Finite element modeling and experimental validation of fretting wear scars in thin steel wires," *Wear*, vol. 289, pp. 26–38, 2012.
[41] P. A. Xu *et al.*, "Elastomeric passive transmission for autonomous force-velocity adaptation applied to 3D-printed prosthetics," *Sci. Robot.*, vol. 3, no. 23, 2018.
[42] Thomson Ind. Inc. CA, USA. Ball Screws and Ball Splines, 2013. [Online]. Available: https://www.thomsonlinear.com/downloads/screws/Ball_Screws_Splines_cten.pdf, Accessed: Jan. 14, 2021.
[43] THK Co., LTD., Tokyo, Japan. Ball screw THK general catalog, 2017. [Online]. Available: https://www.thk.com/sites/default/files/documents/uk_pdf/product/general/a/ee_A15.pdf, Accessed: Jan. 14, 2021.

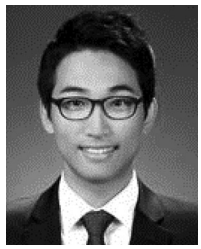

Byungchul Kim (Member, IEEE) received the B.S., M.S., and Ph.D. degrees from Seoul National University, Seoul, South Korea, in 2012, 2014, and 2020, respectively, all in mechanical and aerospace engineering.

He is currently a Postdoctoral Researcher with the Soft Robotics Research Center, Seoul National University, Seoul, South Korea. His research interests include rehabilitation robots, soft wearable robots, and control of assistive devices.

Useok Jeong received the B.S. and Ph.D. degrees from Seoul National University, Seoul, South Korea, in 2010 and 2017, respectively, both in mechanical and aerospace engineering.

He is currently a Senior Researcher of Applied Robot R&D Department, Korea Institute of Industrial Technology, Ansan-si, South Korea. His research interests include cable-driven systems, soft wearable robots, control of assistive devices, and dynamics modeling and control.

Brian Byunghyun Kang (Member, IEEE) received the B.S. degree from Cornell University, Ithaca, NY, USA, in 2010, and the M.S. and Ph.D. degrees from Seoul National University, Seoul, South Korea, in 2013 and 2019, respectively, all in mechanical and aerospace engineering.

He is currently a Postdoctoral Researcher with the Soft Robotics Research Center, Seoul National University, Seoul, South Korea. His research interests include soft wearable robots and AI.

Kyu-Jin Cho (Member, IEEE) received the B.S. and M.S. degrees from Seoul National University, Seoul, South Korea, in 1998 and 2000, respectively, and the Ph.D. degree from the Massachusetts Institute of Technology, Cambridge, MA, USA, in 2007, all in mechanical engineering.

He was a Postdoctoral Fellow with Harvard Microrobotics Laboratory until 2008. He is currently a Professor of mechanical and aerospace engineering, the Director of BioRobotics Laboratory at Seoul National University, and the Director of Soft Robotic Research Center. His research interests include biologically inspired robotics, soft robotics, soft wearable devices, novel mechanisms using smart structures, and rehabilitation/assistive robotics.

Dr. Cho was the Recipient of the 2014 IEEE RAS Early Academic Career Award, 2014 ASME Compliant Mechanism Award, and 2013 KSPE Paik Am Award.